Chemical Geology 270 (2010) 148–163

Contents lists available at ScienceDirect

Chemical Geology

journal homepage: www.elsevier.com/locate/chemgeo

Trace elements record depositional history of an Early Archean stromatolitic carbonate platform

Abigail C. Allwood [a,c,*], Balz S. Kamber [b], Malcolm R. Walter [c], Ian W. Burch [c], Isik Kanik [a]

[a] Jet Propulsion Laboratory, California Institute of Technology, 4800 Oak Grove Dr, Pasadena, CA, 91109, USA
[b] Department of Earth Sciences, Laurentian University, 935 Ramsey Lake Rd, Sudbury, ON, Canada P3E 2C6
[c] Australian Centre for Astrobiology, School of Biotechnology and Biomolecular Sciences, University of New South Wales, Sydney, NSW 2052, Australia

ARTICLE INFO

Article history:
Received 21 January 2009
Received in revised form 31 October 2009
Accepted 19 November 2009

Editor: B. Bourdon

Keywords:
Rare earth element
Archean
Stromatolite
Carbonate
Chert
Pilbara

ABSTRACT

Rare earth elements and selected trace elements were measured in 48 samples of carbonate and chert from stromatolites and associated facies in the 3.45 billion year old Strelley Pool Formation, Pilbara Craton, Western Australia. The samples show coherent REE+Y patterns that vary systematically with sedimentary facies. Chert samples from bedded cherts beneath the Strelley Pool Formation and from the upper bedded chert members in the formation show REE+Y patterns consistent with originating by precipitation from hydrothermal and mixed marine-hydrothermal fluids. In contrast, carbonates and cherts from the stromatolitic reef member share the essential shale-normalized characteristics of other Archean marine precipitates (LREE depletion, positive La and Gd anomalies, absence of a negative Ce anomaly and a strongly superchondritic Y/Ho ratio). The close correspondence between REE+Y signatures and independent sedimentary facies interpretations is viewed as strong evidence for the primary nature of REE+Y patterns. They can thus be used as a proxy for the fluids from which sediments precipitated. Mixing hyperbolae can be constructed that reproduce the chemistry of cherts and carbonates by mixing of hydrothermal and marine fluid endmembers throughout the entire vertical succession from beneath the Strelley Pool Formation to the uppermost cherts. The mixing hyperbolae provide semi-quantitative confirmation that the trace element compositions across the suite of cherts represent different mixtures of ambient seawater and hydrothermal fluids.

Our results indicate that the Earth's oldest supracrustal carbonates and associated cherts record important aspects of the REE geochemistry of the waters in which they precipitated, and provide valuable information on possible habitats of some of Earth's earliest biota.

1. Introduction

Analysis of Earth's earliest fossil record benefits greatly from parallel investigation of the changing sedimentary and chemical environments in which potential biosignatures formed. Most importantly, to interpret the origin of possible biosignatures it is essential to understand the environmental conditions under which they formed. Furthermore, if biosignatures are identified, then knowledge of their environmental context also provides insight to primitive terrestrial ecology and the habitats that nurtured emergent life. Thus, any scientific tool that provides insight to ancient palaeoenvironments is of utmost importance to the study of Earth's earliest fossil and sedimentary rock records.

Rare earth element (REE) chemistry is a valuable tool for investigating early sedimentary palaeoenvironments because the relative abundances of REE in hydrogenous sediments (i.e. autochthonous sediments derived from basin waters) such as carbonate and chert, vary systematically depending on the influence of hydrothermal, terrestrial or marine inputs upon fluids in the basin (e.g. Van Kranendonk et al., 2003; Kamber et al., 2004; Allwood et al., 2006a). Numerous studies have demonstrated that valid proxies of palaeoenvironmental fluid chemistries can be recorded in the trace element composition of Archean hydrogenous sedimentary rocks, including banded iron formation, chert and carbonate (e.g. Bau and Dulski, 1996; Van Kranendonk et al., 2003; Bolhar et al. 2004).

The aim of the present study is to use REE and other trace elements to explore palaeoenvironmental signatures associated with the formation of a stromatolitic carbonate platform in the 3.45 billion year old Strelley Pool Formation, Pilbara Craton, Western Australia. The Strelley Pool Formation contains the oldest supracrustal carbonate deposits on Earth, as well as some of Earth's oldest stromatolites (internally laminated sedimentary structures of probable biological origin: Hofmann, 1973; Awramik et al., 1976). Significantly, it is the oldest formation in the geologic record in which putative fossils can be examined at regional scales, against a relatively well preserved backdrop of sedimentological context that can be correlated across tens of kilometres (Lowe, 1980, 1983; Hoffman et al., 1999; Van

* Corresponding author. Jet Propulsion Laboratory, MS183-301, 4800 Oak Grove Dr, Pasadena, CA, 91109, USA. Tel.: +1 818 393 4275; fax: +1 818 393 4445.
E-mail address: Abigail.C.Allwood@jpl.nasa.gov (A.C. Allwood).

0009-2541/$ – see front matter © 2009 Elsevier B.V. All rights reserved.
doi:10.1016/j.chemgeo.2009.11.013

Kranendonk et al., 2003; Allwood et al., 2006a, 2009). The vertical stratigraphic succession through the Strelley Pool Formation in the study area records a nearly continuous succession of depositional environments before, during and after the formation of the stromatolites, with sedimentary cherts and carbonates present throughout (Allwood et al., 2006a, b, 2007b). That stratigraphy provides a valuable opportunity to use REE and trace element chemistry to investigate the changing palaeoenvironments associated with the development of an Early Archean carbonate platform and some of Earth's oldest putative biosignatures.

Smaller REE datasets from the Strelley Pool Formation were previously reported by Van Kranendonk et al. (2003), and by Allwood et al. (2006a) as part of a suite of contextual features suggesting that the Strelley Pool Formation contains a fossil stromatolite reef formed in a shallow marine setting. Here we present a more detailed analyses of the REE chemistry of sedimentary chert and carbonate in the Strelley Pool Formation and underlying rocks in order to: 1) test the level of detail that can be extracted from the REE chemistry of such Early Archean sedimentary rocks; 2) test the sensitivity and accuracy of microsampling techniques that allow high spatial resolution analysis of sedimentary fabrics; 3) explore the ability of REE to faithfully record intact proxies of changing environmental fluid chemistries in ancient rocks; and, 4) gain detailed insight to the depositional processes associated with the development of Earth's oldest stromatolitic carbonate platform.

2. Background

2.1. Geological setting

The Strelley Pool Formation is a ~30–400 m thick clastic and chemical sedimentary rock formation deposited on the northern Pilbara Craton during a c.80 Myr period from the end of Panorama Formation volcanism at c.3.43 Gyr and onset of Euro Basalt volcanism at c.3.35 Gyr. Previously mapped as part of the Warrawoona Group, the Strelley Pool Formation is now designated as a separate unit between the top of the Warrawoona Group and the base of the Kelly Group in the lower Pilbara Supergroup (Hickman, 2008, and references therein).

Outcrops of the Strelley Pool Formation occur in greenstone belts across the c. 200 km diameter of the East Pilbara Granite-Greenstone Terrane (Van Kranendonk et al., 2002). The present study focuses on the south western Panorama Greenstone Belt in the North Pole Dome (Fig. 1), in an area centred upon a notable stromatolite locality called the 'Trendall Locality', where coniform stromatolites were first identified in the area (Hoffman et al., 1999). Compared to the Strelley Pool Formation in other parts of the Pilbara, outcrops in the south western Panorama Greenstone Belt are relatively well preserved, with widespread preservation of primary carbonate rocks and abundant stromatolites with diverse morphology (Allwood et al., 2007a).

In the study area, the formation consists of a ~30 m thick succession, thickening to over 100 m in the south, deposited over volcano-sedimentary rocks of the Panorama Formation (DiMarco and Lowe, 1989) and altered basaltic rocks of the Mt Ada Basalt. The basal contact of the Strelley Pool Formation in the East Strelley Greenstone Belt c.30 km north of the study area represents a significant period of erosion or non-deposition (Buick et al., 1995; Van Kranendonk et al., 2002). However, in the study area in the southern Panorama Greenstone Belt, the basal contact is disconformable to paraconformable or conformable with the underlying rocks. In some parts of the study area the contact represents only a brief pause between deposition of thinly bedded tuffaceous mudstone of the Panorama Formation and deposition of basal conglomerates of the Strelley Pool Formation (Allwood et al., 2006a).

Four members are recognized from base to top of the Strelley Pool Formation in the study area. Member 1 is a coarse clastic unit 2–3 m thick. Member 2 consists of up to 20 m of millimetre-laminated and bedded stromatolitic dolomite and chert. Member 3 consists of up to 2 m of bedded black and white chert with iron-rich stromatolitic laminites, and member 4 is a unit of volcaniclastic and siliciclastic sedimentary rocks, up to 300 m thick or more (Fig. 2). The Strelley Pool Formation has been variously interpreted as: a restricted subaqueous deposit (Lowe, 1983); a hydrothermal exhalite (Lindsay et al., 2005); or a shallow marine deposit (Van Kranendonk et al., 2003). Allwood et al. (2006a) proposed that the Strelley Pool

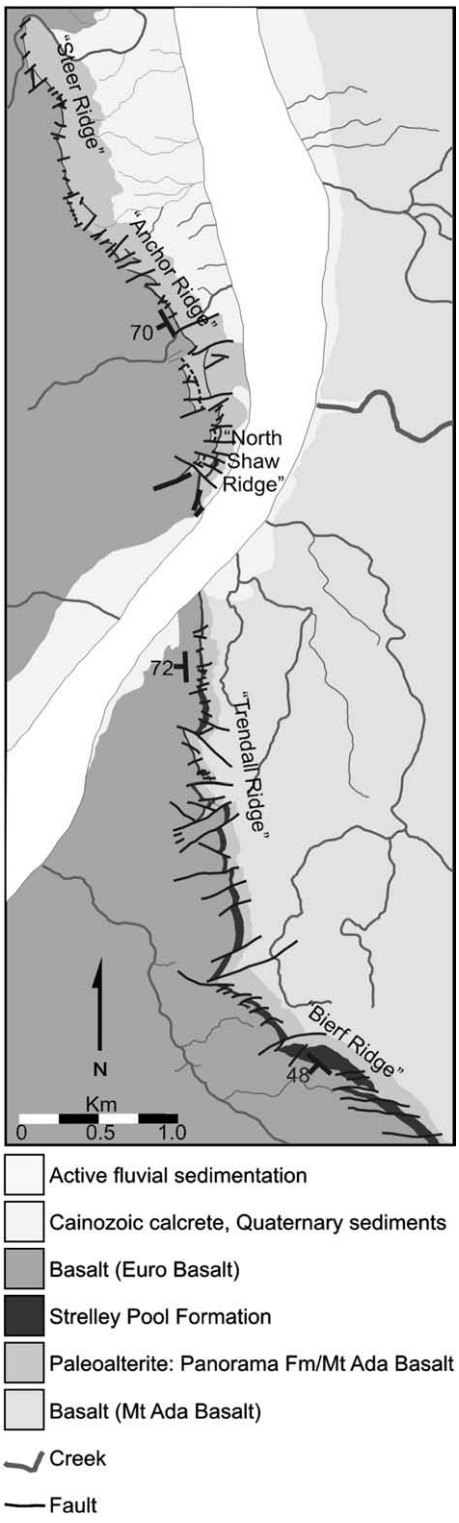

Fig. 1. Simplified geologic map of the Strelley Pool Formation and cross-cutting faults in the study area. Modified from Allwood et al. (2007a).

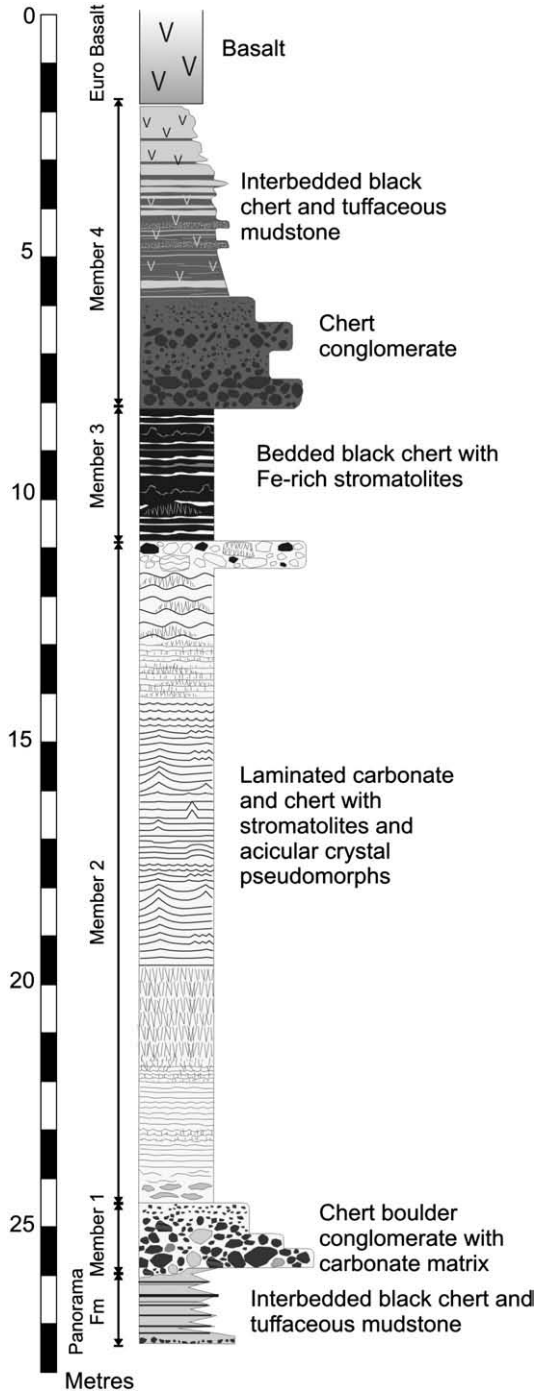

Fig. 2. Representative stratigraphic column of the Strelley Pool Formation in the study area (column located at "North Shaw Ridge"). Reprinted from Allwood et al., 2006, p. 192. Copyright 2006, with permission from Elsevier.

Formation in the study area was deposited in a succession of rocky coastal to isolated peritidal marine carbonate platform reef environments during transgression of previously emergent crust, followed by a period of clastic and volcaniclastic sediment deposition in subsiding fault blocks.

2.2. Samples

Chert or chert–carbonate samples were collected from all members of the Strelley Pool Formation and from the immediately underlying Panorama Formation, covering all major facies deposited immediately before, during and after stromatolite development (Allwood et al., 2006a). The samples were collected from steeply dipping outcrops along "Trendall Ridge", "North Shaw Ridge", "Anchor Ridge" and "Steer Ridge" (Fig. 1): a continuous series of ridges that extends a total of about 4 km north and about 3 km to the south of the "Trendall Locality" (Hoffman et al., 1999). Field samples were collected from the least-weathered parts of the outcrops using a hammer and, where necessary, a hand held power coring drill. Sample context and descriptions are presented in Section 3 and summarized in Table 1.

2.3. Trace elements in hydrogenous sedimentary rocks

The trace element composition of fluids in the depositional environments represented by our samples can be envisaged in terms of three possible endmembers: open marine seawater; coastal/estuary waters under the influence of a terrigenous source (e.g. a river mouth) and hydrothermal fluid. Numerous empirical studies have demonstrated that trace element composition of hydrogenous sediments (formed from dissolved components in the fluid) such as banded iron formation, chert and carbonate record a diversity of environments often representing the interaction of at least two fluid sources (e.g. Bolhar et al. 2004; Van Kranendonk et al., 2003; Bau and Dulski, 1996; Kamber and Webb, 2001). Thus, the trace element composition of the hydrogenous sediments can also be considered in terms of marine, terrestrial and hydrothermal endmembers.

For analytical purposes, the relative abundances of REE+Y in rock and fluid samples are typically normalized to a known shale composite (such as Post Archean Average Shale, or PAAS: Taylor and McLennan, 1985) that is considered to represent average terrigenous input to the hydrosphere from weathering of upper continental crust. Shale-normalized diagrams are useful for highlighting the relative abundance of REE+Y in geological samples.

In shale-normalized relative abundance diagrams, modern seawater is characterized by:

(i) relative depletion of the light REE (LREE) over the heavy REE (HREE) compared to the input source chemistry (e.g. shale);
(ii) a strongly superchondritic Y/Ho ratio, expressed as a prominent positive Y anomaly in the pattern (elemental Y/Ho 40–90; Bau, 1996);
(iii) a strong positive La anomaly (La/La^* typically between 1.3 and 1.5);
(iv) a positive Gd anomaly (Gd/Gd^* typically between 1.15 and 0.30);
(v) a variable but generally well-developed negative Ce anomaly; and possibly
(vi) a small positive Lu anomaly.

These features reflect unique complexation phenomena in the hydrosphere (e.g. Bau, 1999). In contrast to REE in the vast majority of geological materials, REE dissolved in sea, estuarine, and saline ground waters do not display smooth abundance patterns as a function of ionic radius when normalized to their dominant source (shale). Rather, it is now well established that shale-normalized marine, estuarine, and ground water REE patterns show very significant abundance peaks for the elements La, Gd, Y and Ce. Positive La, Gd and Lu peaks are attributed to the higher surface and solution complexation stabilities of those elements (with f-orbital electrons empty, half-filled and full, respectively) relative to neighbouring elements (e.g. Bau et al., 1999). A negative Ce anomaly is observed because Ce, unlike the trivalent REE, is oxidized to Ce(IV) on particle surfaces from which it is less efficiently desorbed (Bau and Koschinsky, 2009). In addition, the element Y, which is a chemical twin of the HREE element Ho (e.g. Bau, 1996), has a very different behaviour in aqueous solutions (Nozaki et al., 1997; Bau and Dulski, 1999) leading to a high Y/Ho ratio compared to all other geological materials, which have an essentially constant Y/Ho ratio. The progressive enrichment of REE as a function of ionic radius (LREE depletion/HREE enrichment) is believed to reflect the cumulative effects of solution complexation with carbonate and surface complexation with hydroxyl groups,

Table 1
Summary of the 48 analyzed samples. "ACA" samples are 2 each (carbonate and chert components bear the same sample number).

Sample	Type	Unit	Location	Description	Parent (field) sample #
AA1	Carbonate	M2 bed 2	N Shaw	Stromatolite—carbonate lamina	12/06/03-5-TES1-1
AA2	Chert	M2 bed 2	N Shaw	Stromatolite—chert lamina	12/06/03-5-TES1-3
AA3	Chert	M3		Bedded black chert with iron-rich laminites	14/06/03-5-TES1-1
AA4	Chert	M3		Black chert clast from iron-rich laminite-encrusted conglomerate	16/06/03-3B-TES1-2
AA5	Carbonate	M1	N Shaw	Carbonate matrix of conglomerate	07/08/03-4-TES1-1
AA7	Chert	M4	N Shaw	Bedded black chert with tuffaceous mudstone layers	12/08/03-8-TES1-1
AA8	Carbonate	M1	N Shaw	Carbonate matrix of conglomerate	
AA10	Chert	Underlying	N Shaw	Bedded/laminated black chert	14/08/03-4-TES1-1
AA11	Chert	Underlying	N Shaw	Bedded/laminated black chert	14/08/03-7-TES1-1
AA12	Chert	Underlying	N Shaw	Bedded/laminated black chert	14/08/03-16-TES1-1
AA13	Chert	Underlying	N Shaw	Bedded/laminated black chert	14/08/03-32-TES1-1
AA14	Chert	Underlying	N Shaw	Bedded/laminated black chert	14/08/03-29-TES1-1
AA17	Chert	M1	N Shaw	Clast #1 (black chert)	14/08/03-21-TES1-1
AA18	Chert	Underlying	N Shaw	Clast #2 (black chert)	14/08/03-21-TES1-2
AA20	Chert	Underlying	N Shaw	Clast #2 (black chert)	14/08/03-24-TES1-3
AB4	Carbonate	M2 bed 1	Anchor	Grainy lamina from boulder-encrusting laminae	13.08.04-24-TES1-4
AB5	Carbonate	M2 bed 1	Anchor	Grainy lamina from boulder-encrusting laminae	13.08.04-24-TES1-5
AB6	Carbonate	M2 bed 1	Anchor	Fenestral/flat laminae/evaporite crystal pseudomorphs (lamina 1)	130804-3-TES1-4
AB7	Carbonate	M2 bed 1	Anchor	Fenestral/flat laminae/evaporite crystal pseudomorphs (lamina 2)	130804-3-TES1-5
AB8	Carbonate	M2 bed 1	Anchor	Fenestral/flat laminae/evaporite crystal pseudomorphs (lamina 1)	130804-3-TES1-6
AB9	Carbonate	M2 bed 1	Anchor	Fenestral/flat laminae/evaporite crystal pseudomorphs (lamina 2)	130804-3-TES1-7
AB12	Chert	M3	N Shaw	Bedded black chert: with iron oxide laminae	010904-10-TES1-1
AB13	Chert	M4	N Shaw	Black vein chert: phreatomagmatic breccia matrix	010904-11-TES1-1
AB14	Chert	M4	N Shaw	Bedded black chert with tuffaceous mudstone layers	010904-15-TES1-1
AB15	Chert	M4	N Shaw	Bedded black chert with tuffaceous mudstone layers and ripples	010904-16-TES1-1
AB16	Chert	M3	N Shaw	Bedded black chert: with iron oxide laminae	010904-30-TES1-1
AB17	Chert	M4	N Shaw	Bedded black chert with tuffaceous mudstone layers	010904-33-TES1-1
AB18	Chert	M4	N Shaw	Bedded black chert with tuffaceous mudstone layers	010904-34-TES1-1
ACA 1	Carbonate	M2 bed 1	N Shaw	Upward transect at NS ridge: lowest	01.09.04-24-TES1-1
ACA 2	Carbonate	M2 bed 1	N Shaw	Upward transect at NS ridge: middle	01.09.04-25-TES1-2
ACA 3	Carbonate	M2 bed 1	N Shaw	Upward transect at NS ridge: highest	01.09.04-26-TES1-3
ACA 4	Carbonate	M2 bed 1	N Shaw	Encrusting/domical stromatolite: 2 cm above boulder	13.08.04-2-TES1-1
ACA 5	Carbonate	M2 bed 1	N Shaw	Encrusting/domical stromatolite: 10 cm above boulder (cherty lamina)	13.08.04-2-TES1-2
ACA 6	Carbonate	M2 bed 1	Anchor	Fenestral carbonate: evaporite crystal pseudomorphs	13.08.04-3-TES1-1
ACA 7	Carbonate	M2 bed 1	N Shaw	Fenestral carbonate: matrix between evap. crystal pseudomorphs	13.08.04-3-TES1-2
ACA 8	Carbonate	M2 bed 1	N Shaw	Fenestral carbonate: flat laminae	13.08.04-3-TES1-3
ACA 9	Carbonate	M2 bed 2	Anchor	Laminae from wrinkly sided stromatolite	26.07.04-3-TES1-1
ACA 10	Carbonate	M2 bed 2	Trendall	Flat laminite with granular fabric and desiccation cracks	IB04-2-TES1-1
ACA 1	Chert	M2 bed 1	N Shaw	Upward transect at NS ridge: lowest	01.09.04-24-TES1-1
ACA 2	Chert	M2 bed 1	N Shaw	Upward transect at NS ridge: middle	01.09.04-25-TES1-2
ACA 3	Chert	M2 bed 1	N Shaw	Upward transect at NS ridge: highest	01.09.04-26-TES1-3
ACA 4	Chert	M2 bed 1	N Shaw	Encrusting/domical stromatolite: 2 cm above boulder	13.08.04-2-TES1-1
ACA 5	Chert	M2 bed 1	N Shaw	Encrusting/domical stromatolite: 10 cm above boulder (cherty lamina)	13.08.04-2-TES1-2
ACA 6	Chert	M2 bed 1	Anchor	Fenestral carbonate: evaporite crystal pseudomorphs	13.08.04-3-TES1-1
ACA 7	Chert	M2 bed 1	N Shaw	Fenestral carbonate: matrix between evap. crystal pseudomorphs	13.08.04-3-TES1-2
ACA 8	Chert	M2 bed 1	N Shaw	Fenestral carbonate: flat laminae	13.08.04-3-TES1-3
ACA 9	Chert	M2 bed 2	Anchor	Laminae from wrinkly sided stromatolite	26.07.04-3-TES1-1
ACA 10	Chert	M2 bed 2	Trendall	Flat laminite with granular fabric and desiccation cracks	IB04-2-TES1-1

which both increase in stability with atomic number (Sholkovitz and Schneider, 1991; Lee and Byrne, 1992). Studies of REE behaviour across the salinity barrier of estuaries have demonstrated the development of these features at relatively low salinities (e.g. Lawrence and Kamber, 2006; Kulaksiz and Bau, 2007).

In open marine environments away from significant direct terrigenous or hydrothermal inputs, the hydrogenous sediment carbonate, chert and phosphate inherit the distinctive REE features of open seawater. Unless affected by secondary REE exchange during lithification and subsequent geologic overprint, these features are also passed on to chemical sedimentary rocks. Preservation of seawater REE signatures in hydrogenous marine sediments has been widely documented throughout the geological record and, significantly, essentially the same suite of features (excepting the redox-sensitive Ce anomaly) have been documented in Early Archean chemical sedimentary rocks including carbonates, cherts and banded iron formation (Derry and Jacobsen, 1990; Alibert and McCulloch, 1993; Sugitani, 1992; Bau and Moller, 1993; Kamber and Webb, 2001; Van Kranendonk et al., 2003; Kamber et al., 2004; Nothdurft et al., 2004; Alexander et al., 2008). The presence of marine REE characteristics in Archean sedimentary rocks indicates that the REE elemental cycle, which requires land, rivers, estuaries, oceans and hydrothermal vents was operational in the Early Archean. However, there are also some notable differences in Archean marine hydrogenous sediments, which provide insights to the redox conditions and ocean chemistry of the Early Archean Earth. The absence of a negative Ce anomaly (related to the redox behaviour of that element) in Archean carbonates is interpreted to reflect deposition under anoxic conditions in the Archean ocean. The strong positive Eu anomaly observed in Archean marine precipitates is *prima facie* evidence that at least the deep ocean was anoxic and that high T hydrothermal solutions were a very significant input source of REE (e.g. Derry and Jacobsen, 1990; but see also Kamber and Webb, 2001). In the shallow marine environment, where deeper sourced waters mix with shallow water with a more local, riverine dominated chemistry, the extent of the Eu anomaly can co-vary with other features of the REE pattern and with radiogenic isotope composition (e.g. Kamber and Webb, 2001). In these instances, the extent of the Eu anomaly can be a proxy for depositional environment, chiefly relative water depth.

The trace element chemistry of hydrothermal fluids varies as a function of the physical and chemical conditions associated with seafloor alteration and venting of the fluids into the ocean. The physical and chemical conditions in the hydrothermal system exert

control over the extent of fluid–rock interaction; the complexation of trace elements by ligands; the precipitation and separation of secondary phases (Klinkhammer et al., 1994; Douville et al., 1999), and (in mid ocean ridge and back arc spreading centre environments) diagenetic redox reactions at the sediment–basalt interface (Wheat et al., 2002). Clearly, of all REE sources to the sedimentary environment of interest in this study, hydrothermal fluids are the least well understood, even in the present Earth. However, some common factors of high temperature hydrothermal fluids (>250 °C) are recognized. In diagrams normalized to mid ocean ridge basalt (MORB), high T hydrothermal fluids are enriched in LREE and Eu; have higher concentrations of REE overall when compared to seawater; and have chondritic Y/Ho ratios (e.g. Klinkhammer et al., 1994; Bau and Dulski, 1999). Low T hydrothermal solutions (<250 °C) are not as well studied as high T solutions, but essentially share REE characteristics with high T solutions. However, Wheat et al. (2002) argue that REE in low T solutions undergo fractionation due to the formation of secondary oxides and carbonates, mobilization of some elements in the sediment pile and formation of albite in basalt. Thus, a LREE-enriched pattern with chondritic Y/Ho ratios would be consistent with origins in a high T hydrothermal system comparable to modern mid ocean ridge or back arc spreading centre systems. But there is scope for diversity among REE patterns of hydrogenous sediments formed in ancient hydrothermal systems.

In sedimentary basins affected by terrigenous influx (i.e. crustal or shale contamination) the composition of hydrogenous sediments is a mixture of originally colloidal and particulate components. If particulate components are significant, they have a strong effect on the trace metal concentrations. Strictly terrigenous contamination is best recognized by increased trace element concentration, and covariation trends between REE features and Th, Zr, Ga or Sc (all elements concentrated in continental detritus by several orders of magnitude compared to seawater and hydrothermal fluids). Clastic contamination has a strong tendency to flatten the shale-normalized REE patterns, provided that the shale composite is a valid approximation of terrigenous input into the particular environment of the studied rocks. In that regard, recent studies have demonstrated the importance of understanding the trace element composition of the crust in the hinterland area and – by implication – the trace element chemistry of terrigenous influx to the basin (Kamber et al., 2004). In the present study, a modern alluvial sediment composite from north eastern Australia (Mud of Queensland, "MuQ") was used as the normalization factor. These sediments reflect a bi-modal erosion source in NE Australia composed of strongly weathered basaltic rocks and Proterozoic granitoids. For this reason MuQ has some validity as an approximation of the composition of sedimentary deposits formed in Early Archean granite-greenstone terrains. In addition, the data for MuQ (Kamber et al., 2005) were obtained with exactly the same analytical method as this dataset and MuQ also contains accurate and precise data for mono-isotopic Pr, Tb, Ho and Tm, which facilitate accurate assessment of La, Eu, Y and Gd anomalies.

3. Sedimentary context and mineral paragenesis

3.1. Underlying unit, member 1, member 3 and member 4 chert samples

The underlying Panorama Formation strata consist of a thin (up to 5 m thick), bedded unit that thickens, thins and pinches out along strike in the study area. The unit has a variable character but is typified by thinly bedded to laminated volcaniclastics and chert showing graded bedding (volcaniclastics grading up into chert) and cross lamination (Fig. 3i). The sampled outcrop also has metre-thick beds of massive black chert (Fig. 3j) and coarse conglomerate layers. Samples were collected from the thick black chert beds, and from chert clasts in the conglomerate layer. Some of the chert clasts in the conglomerate layers have jasper banding, indicating erosion from a unit that locally subcrops the Panorama Formation in the area, and is most likely the Marble Bar Chert.

Member 1 of the Strelley Pool Formation also thickens, thins and pinches out along strike, and varies from bedded conglomerate with carbonate matrix to large, isolated and clustered boulders with no matrix. Soft-deformed clasts of the underlying volcaniclastics occur locally in the conglomerate (Allwood et al., 2006a, 2007b). The sampled outcrop consists of bedded conglomerate with a brownish carbonate matrix (Fig. 3f) that contains finely disseminated clays. The carbonate matrix is contiguous with the overlying member 2 carbonate, but the latter is blue-grey and contains no clastic material.

Member 3 consists of layered black chert with thin, discontinuous white chert laminae (Fig. 3c) and thin beds of laminated hematite that forms stromatolitic domes, cm-high columns and wrinkled layers ("iron-rich laminite" stromatolites of Allwood et al., 2006a) (Fig. 3b). The chert contains rare silicified acicular crystal beds and crystal fans, and pebble conglomerate layers, some with channel fill geometry. Samples were taken from black chert away from any clastic material, crystal pseudomorphs or iron-rich laminites. Member 4 consists mainly of bedded black chert with clastic and volcaniclastic layers. Locally, the bedded strata pass laterally into a breccia consisting of silicified tuffaceous mudstone clasts in a black chert matrix (Fig. 3a). Samples were collected from thick, massive black chert beds away from mudstone layers, and from the black chert breccia matrix.

In thin section, black cherts from members 3 and 4, and from the underlying Panorama Formation have diverse microfabrics consisting of carbonaceous particles (clots, clasts, diffuse particles) and/or layers (thin films and stringers) in a matrix of microcrystalline to mesocrystalline quartz (Fig. 4). In all chert members there is a complex post-depositional silica emplacement history. However, the chert that forms the matrix of the organic material appears to be primary in origin and is cross-cut by all other "generations" of translucent, organic-free silica (Fig. 4a). Significantly, the emplacement of secondary silica evidently began in the very near subsurface, before the black chert was fully lithified. This is evident in places where the bedded black chert (c1) exhibits soft-sediment deformation where it is intruded by the youngest translucent silica phase (c2) (Fig. 4a, d).

3.2. Member 2 samples

Member 2 contains diverse facies, including seven types of stromatolite and acicular crystal pseudomorphs, possibly after aragonite. The lithology throughout member 2 consists of dolomite and chert, interlaminated or otherwise closely associated on the millimetre-scale. The carbonate and chert are variably recrystallized and there is local evidence for multiple phases of post-depositional silicification, particularly in association with cross-cutting chert veins (Van Kranendonk and Pirajno, 2004). Samples were collected from

Fig. 3. Outcrop photographs and slab images of carbonate and chert facies analyzed in the study, showing unit of origin and sample number (where relevant). (a) Upper part of member 4 in outcrop, showing phreatomagmatic breccia consisting of pale grey-green silicified tuff clasts in a matrix of black (organic rich) chert. (b) Member 3 in outcrop, showing black chert with red, iron-rich laminites encrusting chert clasts. (c) Member 4 in outcrop: massive to faintly bedded/laminated black chert with thin, intrusive layers of white chert. (d) Member 2 bed 1: encrusting/domical stromatolite polished slab showing detail of chert (dark) and carbonate (light) laminoid fabric. (e) Member 2 bed 1 polished slab showing multiple fabrics. The upper part shows an irregular laminoid fenestral fabric in which fenestrae are filled with chert. The dark layers exhibit local small clusters of acicular, radiating crystals (e.g. above black arrow at lower right). (f) Member 1 breccia/conglomerate: cut slab showing chert and carbonate clasts in a brown, carbonate matrix. (g) Member 2 bed 2, polished slab showing flat laminated dolomite (light) and chert (dark). (h) Member 2 bed 2, polished slab showing a cross section view of chert–dolomite laminae on the side of a coniform stromatolite. Apex of stromatolite is to the right. (i) Underlying unit (Panorama Fm) outcrop showing thinly bedded black chert and pale grey-green silicified tuff. (j) Underlying unit (Panorama Fm) outcrop showing massive black chert.

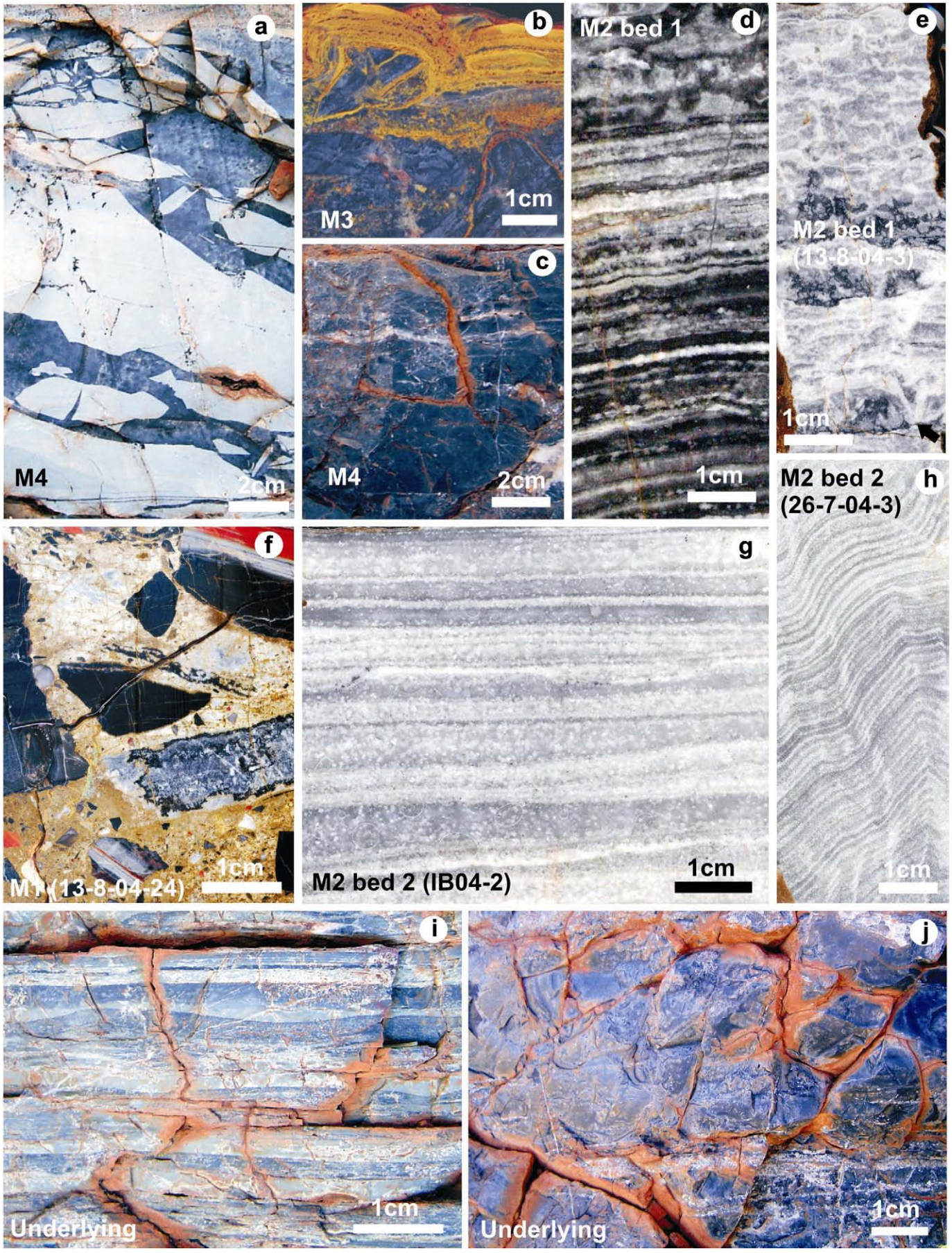
a
M4
2cm
b
M3
1cm
c
M4
2cm
d
M2 bed 1
1cm
e
M2 bed 1
(13-8-04-3)
1cm
f
M1 (13-8-04-24)
1cm
g
M2 bed 2 (IB04-2)
1cm
M2 bed 2
(26-7-04-3)
h
1cm
i
Underlying
1cm
j
Underlying
1cm

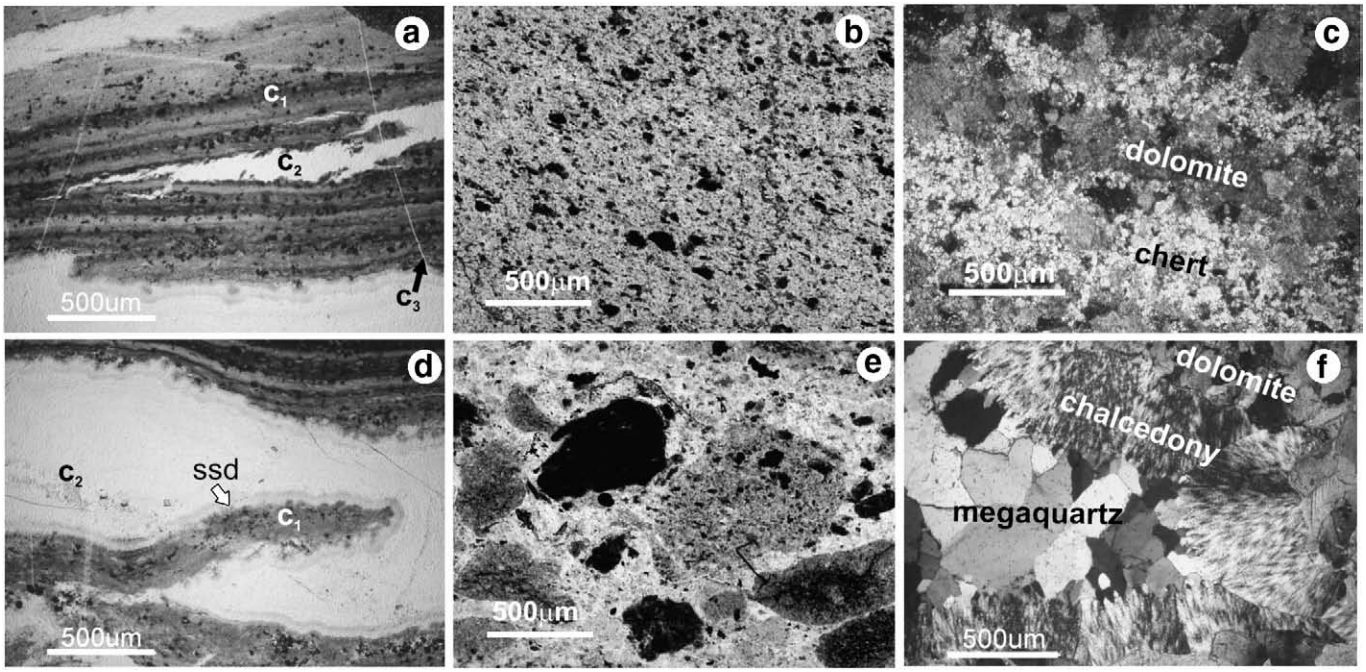

Fig. 4. Photomicrographs of black cherts in thin section. (a) Member 3 black chert showing water-sorted texture of organic materials in silica matrix (c1), later intruded by two translucent silica phases, c2 and c3 (plane polarized light). (b) Panorama Formation black chert, comprising grains of organic matter in a chert matrix. Note preferred orientation of grains parallel to bedding (plane polarized light). (c) interlaminated dolomite and chert in member 2 stromatolite (cross polarized light). (d) Member 3 black chert showing soft-sediment deformation (ssd) where the earliest (sedimentary) chert is intruded by early diagenetic silica (c2) (plane polarized light). (e) Member 4 black chert showing a variety of carbonaceous clasts in a chert matrix (plane polarized light). (f) Cavity-fill texture in member 2 chert lamination (cross polarized light).

parts that exhibit well preserved relict sedimentary textures, away from veins and late diagenetic silicification.

In thin section, carbonate and chert are intimately associated, and there are almost no pure chert or carbonate laminae, only chert-rich and carbonate-rich laminae. Significantly, the lower contact of member 2 marks a sudden complete disappearance of any clastic material: this has been interpreted as evidence of the drowning of a low-relief isolated landmass and onset of fully marine conditions away from any significant source of erosional (terrigenous) input (Allwood et al., 2006a, 2007a, b).

The carbonate is almost entirely dolomite, although small inclusions of calcite are present in the chert-rich laminae. The dolomite consists mainly of roughly equigranular, anhedral crystals in a sutured mosaic (Fig. 5a, d), which is consistent with moderate to advanced dolomite recrystallization. Very fine grained (~2 μm) dolomite is locally abundant, occurring around the margins of some crystals and at contacts between chert and dolomite laminae (Fig. 5c, d). The fine grained dolomite is closely associated with organic matter, suggesting that organic matter may have played a role in its formation. Cross-cutting relationships indicate that these latter two dolomite fabrics developed multiple times during diagenesis. A third type of dolomite occurs locally, and consists of equigranular, euhedral dolomite rhombs, or partial rhombs, with crystal growth zones (Fig. 5b). The rhombs commonly occur at the margins of chert-filled laminoid fenestrae, protruding into the chert in a manner that suggests they are non-replacive, early diagenetic overgrowths, and that they have not been overprinted by recrystallization since their formation. In summary, most of the dolomite is neomorphic and possibly replacive after calcite or aragonite and some dolomite (D3) probably formed as a non-replacive, early diagenetic precipitate, but there appears to have been no significant replacement of non-carbonate phases.

The term chert is used broadly here, to include lithologies containing microcrystalline quartz as well as mesocrystalline quartz. The microfabric of chert laminae is variable but consists mainly of mesocrystalline quartz with undulose extinction and crenulate crystal boundaries (Fig. 4c). Many chert laminae in the lower part of bed 1/member 2 show void-fill fabric with wall-coating isopachous cements, megaquartz or chalcedony infill (Fig. 4f).

Van Kranendonk and Pirajno (2004) proposed that cherts in the Strelley Pool Formation are hydrothermal in origin, and the finely laminated chert in member 2 formed when hydrothermal silica intruded along laminae, replacing carbonate. However, field observations made in this study indicate that this latter interpretation cannot be universally applied to laminated silica throughout member 2. Rather, chert veins typically have a cross-cutting relationship to the laminated silica in member 2, and continue to cross-cut all the way to the upper members of the formation. Sedimentary fabrics in the chert, particularly cavity-fill fabrics (Fig. 4f) are clearly diagenetic in origin. However, studies of recent sedimentary (non-skeletal) silica show that such diagenetic fabrics also form in sedimentary silica (Jones and Renaut, 2007) through early burial transition from the primary non-crystalline silica (opal-A: SiO_2nH_2O) to opal-CT, opal-C and ultimately quartz (e.g. Kastner et al., 1977; Smith, 1998; Herdianita et al., 2000; Lynne et al., 2005). The process involves dissolution–reprecipitation reactions that heterogeneously alter the primary fabrics, creating porosity; preferentially altering some elements of the original fabric; and releasing Si and O into solution, which can then be re-precipitated elsewhere in the sediment pile (Jones and Renaut, 2007), effectively creating secondary silica deposits in the sediment pile. Further recrystallization occurs during burial diagenesis. The fabrics in the Strelley Pool Formation could therefore be interpreted as a heterogeneous mixture of diagenetic quartz fabrics formed in silica laminae that were originally deposited at the sediment–water interface. Thus, there is no field or petrographic evidence that proves a replacive (hydrothermal) origin for the silica.

4. Experimental procedure

Hand-specimens were slabbed with a diamond saw, and the cut surfaces were lightly polished and studied with a hand lens to identify

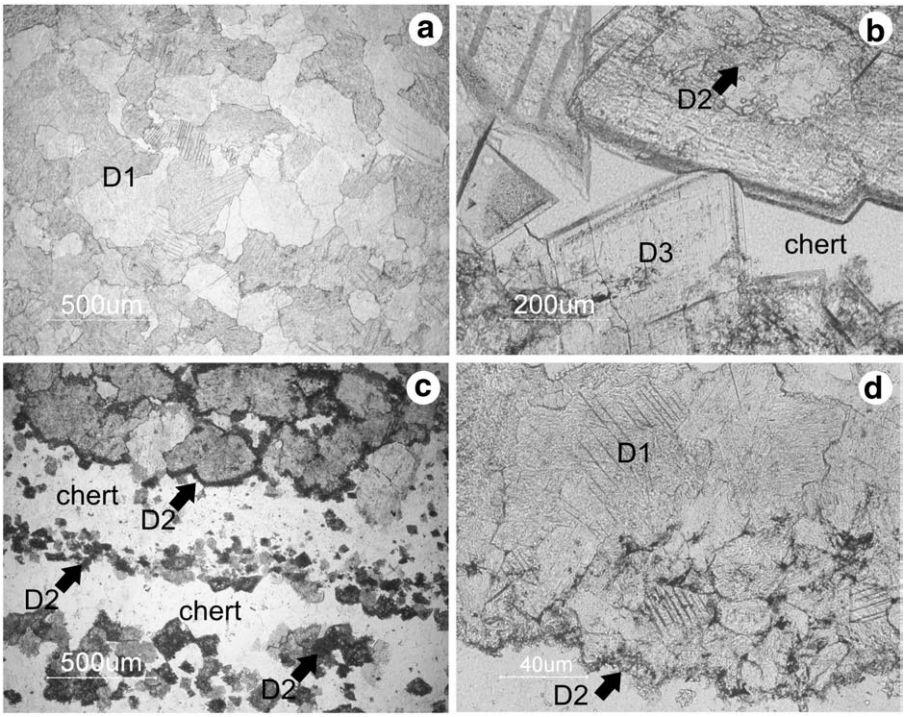

Fig. 5. Photomicrographs showing dolomite microfabrics in thin section (plane polarized light). (a) D1 dolomite. (b) D2, D3 dolomite and chert. (c) D2 dolomite at margins of larger dolomite crystals. (d) D2 dolomite at contact between dolomite and chert laminae.

areas free of weathering. At least one thin section was made for each field sample and examined under a petrographic microscope to determine mineralogy and diagenetic history. Sub-samples for trace element analysis were extracted from the slabs by two different techniques. Most samples were acquired by shattering the slab, or part of the slab, with a 70 ton low-contamination rock press at the ACQUIRE laboratory, University of Queensland, and then retrieving rock shards from the desired part of the slab with clean tweezers. Care was taken to avoid surfaces that had been touched by the diamond saw. Where more precise targeting of sub-samples was required, a low-contamination stainless steel scalpel was used to scrape away the surface of the sample. The new surface was then cleaned and some more sample material was scraped from the fresh rock beneath. Using this technique we were able to collect microgram-sized samples from individual laminae and other millimetre-scale targets with high precision. The samples were prepared for solution ICPMS analysis in the following manner.

Carbonate samples: The samples were submersed in Milli Q water and heated overnight. The water was decanted and samples were triple-rinsed in Milli Q water. The carbonate fraction was dissolved with 2% double-sub-boiling distilled nitric acid on a hotplate at around 130 °C for about 6 h. The carbonate solution was then temporarily decanted into centrifuge tube and a couple of drops of water were used to get remnant solution off the solid chert residue. The chert solids were removed from the beaker, then dried and weighed to determine the amount of carbonate removed. The decanted carbonate solution was then returned to the Teflon beaker and left on the hotplate overnight to dry down the nitrates. The solid was then diluted to the desired volume in 2% nitric acid with internal standards.

Chert samples: After heated washing (as above) and complete carbonate digestion (where carbonate was present in the sample) the chert was rinsed 3 times in Milli Q water, oven dried at 60 °C for 1 h and then weighed. The chert was then dissolved in ultra-clean hydrofluoric acid on a hot plate at around 130 °C for half a day (including 10 min in an ultrasound bath to disturb fluorite precipitates, which can form a protective gel over the sample and hinder complete dissolution). The digests were then dried down on a hotplate (around 120 °C) overnight. Aliquots of 6% HNO_3 were added to the solids at approximately half hour intervals (allowing the sample to dry on hotplate at 110 °C between each aliquot), to convert to nitrates and drive off Si as the tetrafluoride. This yielded a small solid residue whose physical size was used as an approximate guide to the desired dilution in 2% HNO_3 (i.e. attempting to dilute with as little 2% HNO_3 as possible to improve detection limits).

The general ICPMS experimental procedure is an adaptation of that of Eggins et al. (1997), with modifications detailed in Kamber et al. (2003). The instrument used was a Thermo Electron X Series, operated with Xs cones, yielding a sensitivity of 0.3 to 0.4 GHz ppm^{-1} in the REE mass range. Long-term reproducibilities for the period of this study (2004–2005) for USGS and JGS standards were reported in Table 1 of Marx et al. (2005). Instrument response was calibrated against dissolutions of USGS dolerite W-2 (preferred values also reported in Table 1 of Marx et al. (2005)). The only three significant differences between routine analyses and the analyses reported here are the high apparent dissolved solids of the chert solutions (which in reality are much lower because of loss of Si as SiF_4); the reduced number of analytes measured in the carbonate micro-samples (to reduce analysis time and preserve sample); and the use of a 200 instead of 400 µl min^{-1} nebulizer for the smallest samples (to preserve sample). Data are reported in Appendix A. REE were normalized with MuQ in all diagrams.

5. Experimental results

Between each member, the sedimentary rocks of the Strelley Pool Formation show conspicuous variations in REE+Y relative abundance patterns. But *within* each member, variations are less pronounced. The

data are first reported in stratigraphic context, then discussed in the following sections.

5.1. Underlying cherts

Beds of laminated and massive black chert underlying the Strelley Pool Formation are typified by: 1) light REE (LREE) depletion; 2) a positive Eu anomaly that persists with normalization to MuQ, PAAS and a mafic pelite composite; and, 3) a negative Y anomaly (although AA12 and AA14 have a very small positive Y anomaly). Four of the five samples show a positive La anomaly (Fig. 6a).

5.2. Member 1

Chert clasts within member 1 show similar REE characteristics to the underlying cherts (Fig. 6b), particularly the LREE depletion, positive Eu anomaly, negative Y anomaly and absent or slightly positive La anomaly. The patterns of the clasts are particularly similar to one of the underlying cherts, AA13. The carbonate matrix of member 1 (Fig. 6c) is depleted in LREE and has a weak positive Eu anomaly and high MREE/HREE. Notably, the concentrations of REE+Y in the carbonate matrix (particularly AA8) are very high and approach those of MuQ.

5.3. Member 2

All carbonate and chert samples analyzed from member 2 beds and laminae show the essential combination of features typical of Archean seawater, namely: 1) relative depletion of the LREE over the HREE (Pr/Yb of $\ll 1$); 2) a strongly superchondritic Y/Ho ratio (>30); 3) a strong positive La anomaly (30–50% when considered relative to a projection from Nd and Pr); 4) a positive Gd anomaly (15–30% relative to Dy and Sm, instead of Eu, which is itself variable); and 5) a positive Eu anomaly (Fig. 6d, e). A notable feature is that the absolute abundances of REE+Y are typically about 250 times greater in dolomite than in associated chert in the same samples (Fig. 6f).

5.4. Member 3

Chert samples from member 3 have variable chemistry, but seawater characteristics are generally lacking or more poorly developed than in M2 cherts (Fig. 6h). LREE depletion is only slight in three of the four samples, positive La and Y anomalies are present but weak, positive Gd anomalies are virtually absent in all samples. Positive Eu anomalies are present in all four samples.

5.5. Member 4

Cherts from member 4 show much less internal variability than the sample suites from the other members and lack the essential combination of seawater characteristics. The member 4 cherts are characterized by: no significant LREE or HREE depletion; a strong positive Eu anomaly; and a weak negative Y anomaly (Fig. 6i).

The results of four analyses taken at close spacing from two laminae in a member 2 carbonate–chert laminite sample are shown in Fig. 6g. Virtually identical patterns with essential seawater characteristics are observed across the four analyses.

6. Analysis and discussion

6.1. Nature and origin of the REE characteristics

A combination of factors suggests that the REE characteristics of the carbonate and chert samples are neither experimental artifacts nor late diagenetic alteration products, but represent reliable proxies for palaeoenvironmental fluid chemistry. Firstly, the consistency of the REE+Y abundance patterns of the four closely-spaced analyses in a sample of member 2 laminite indicates that false variability is not introduced by the experimental procedure or instrumentation. These patterns were obtained from very small sample sizes (sub-milligram), showing that there is consistency in trace element systematics of the dolomite. It is also important to recall that the chemical separation of mineral phases in the samples prior to their analysis suggests that the detected chert composition is not simply the result of carbonate inclusions—but rather the inherent trace element chemistry of the chert. The high degree of consistency (and seawater origin) of REE signatures in the closely-spaced laminite analyses (Fig. 6g) also indicates that the micro scratch-sampling technique that was used to acquire those and other sub-milligram-sized samples (0.006 to 0.6 milligram) did not introduce significant contamination and has successfully detected geological signatures from extremely small quantities of rock.

Secondly, textural and contextual evidence permit that the dolomite and chert originated as sedimentary silica and carbonate: that is, there is no sedimentological or geochemical evidence that the dolomite and chert are late stage, replacive (e.g. hydrothermal) phases. Sedimentary silica and carbonate would have originally incorporated some chemical imprint of the depositional environment. Importantly, previous studies demonstrate that primary REE characteristics can withstand high water:rock ratio interactions (e.g. recrystallization, dolomitization) due to the typically low concentration of REE in formation fluids (Banner and Hansen, 1990; Bau and Alexander, 2006). Thus, although the chert and dolomite are both recrystallized, and carbonate has been dolomitized, it is reasonable to assume that the REE characteristics of the silica and carbonate have not changed substantially through diagenesis. Preservation of the trace element chemistry during diagenesis and sedimentary reworking is further demonstrated in member 1 conglomerate, where very different REE+Y patterns occur in clasts and matrix. This is consistent with the notion that the chert clasts were eroded from the underlying chert units (some of which have similar REE+Y patterns to the two analyzed clasts) and retained their original REE characteristics to the present day.

Finally, variations in REE+Y characteristics through the studied succession are consistent with sedimentological indicators of the palaeoenvironment (Allwood et al., 2006a, 2007a). Thus, it is reasonable to propose that the REE characteristics – although they reside in diagenetically altered rocks – have survived diagenesis and are reliable proxies for palaeoenvironmental chemistry.

Only member 2 samples consistently show the full suite of REE+Y characteristics of well established Archean hydrogenous marine sediments (e.g. Bolhar et al., 2004). The combination of positive Y, Gd and La anomalies and LREE depletion – rather than the occurrence of any single feature – in both carbonate and chert phases of member 2 indicates their marine origin. These REE characteristics are extremely unlikely to have been produced by circulation of seawater through originally non-marine sediments, and fortuitous reproduction of the seawater REE anomalies by original precipitation from fluids of a completely non-marine origin is equally improbable as those characteristics form by complex and unique natural processes (e.g. Bau, 1999). The REE data (and field observations) are not consistent with previous interpretations, in which it was proposed that all the chert laminae were formed by intrusion of hydrothermal silica along the laminae, replacing carbonate (Van Kranendonk and Pirajno, 2004). Neither are the REE data consistent with precipitation of the carbonate and chert from hydrothermal fluids, like those circulating through hot ocean floor rocks. There is little doubt based on field, petrographic and trace element data that the analyzed samples in member 2 precipitated from seawater in a marine sedimentary environment.

Although chert beds immediately below the Strelley Pool Formation show LREE depletion, they do not show all the essential

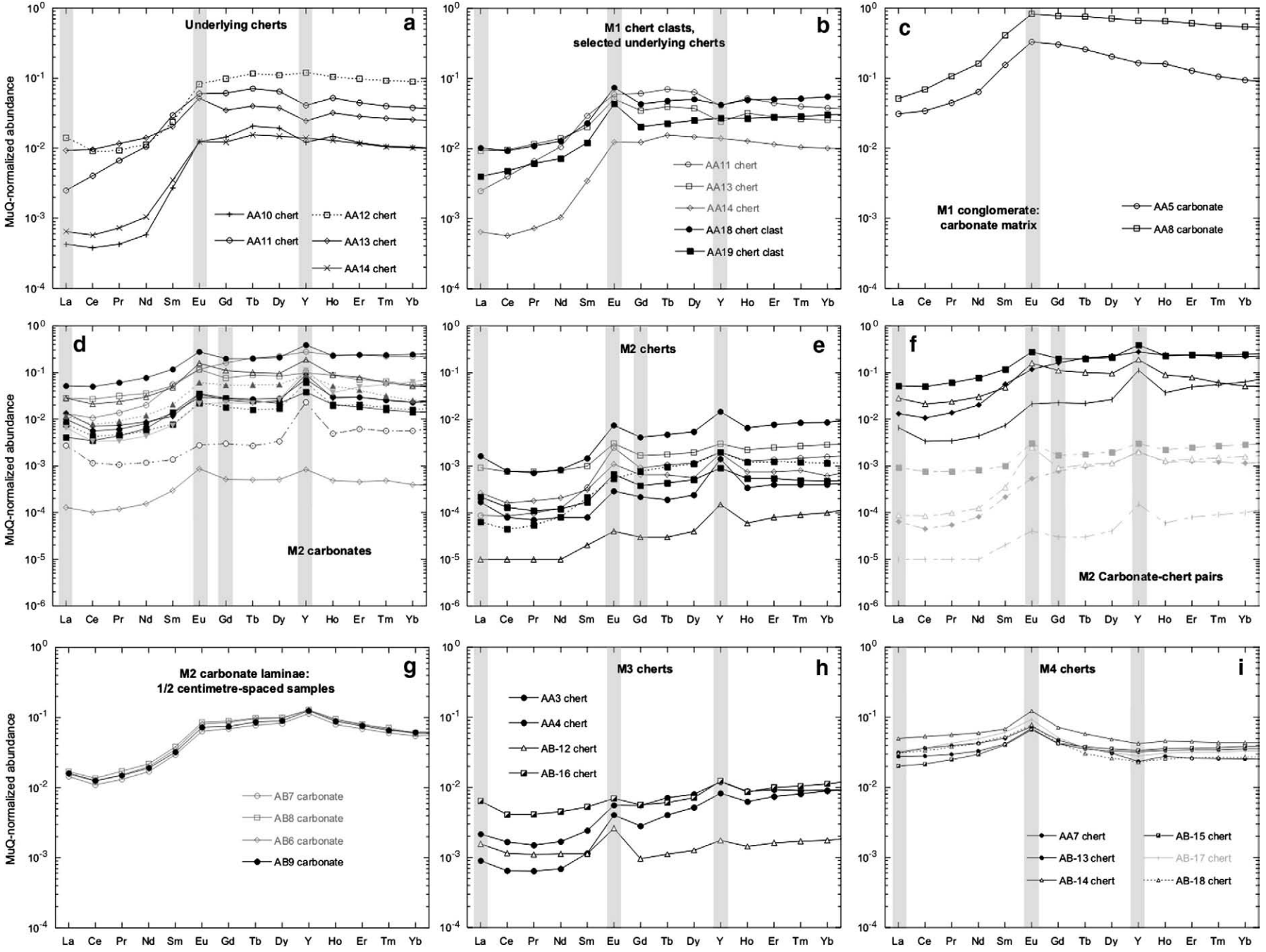

Fig. 6. MuQ-normalized abundances of REE+Y in cherts of the Strelley Pool Formation and underlying rocks.

seawater characteristics. Neither do they show the flat pattern that would indicate significant shale (terrigenous) contamination. The type of pattern of REE+Y relative abundances in the underlying cherts suggests a hydrothermal input. Similarly, the relative abundances of REE+Y in member 3 cherts suggests that there may have been some seawater characteristics in the fluids from which they were derived, but the samples also appear to have been variably influenced by non-marine fluids. The REE+Y characteristics of member 4 cherts are distinct from any of the other units, and are consistent with precipitation from fluids of mixed marine-hydrothermal influence.

Hydrothermal input to members 3 and 4 seems reasonable given that black chert veins cross-cut the underlying strata and terminate locally within member 3 and particularly member 4. It is unclear whether veins also terminate in the underlying Panorama Formation strata, which have limited exposure. The veins would have carried fluids that either vented at the paleosurface or infiltrated the sediment pile, as appears to be the case in some areas of phreatomagmatic brecciation in member 4 (Fig. 3a). Either scenario would present an opportunity for mixing of hydrothermal and seawater chemistries.

6.2. Trace element mixing for variations in chert composition

Given that no significant false signal variations were introduced to the dataset through any of the sampling and analytical procedures – as evidenced by the high reproducibility of results – even small variations between samples may reflect the inherent chemistry of the rocks and relate to variations in the primary composition of the sediments. Therefore, analysis of the more subtle variations in trace element chemistry can be undertaken to test the hypotheses for their origins; namely, the interplay of hydrothermal, marine, and/or terrigenous chemical influences in the palaeoenvironment. These analyses will also further test the hypothesis that sample chemistry has been affected by diagenesis.

Chert is common to all stratigraphic sub-units in the Strelley Pool Formation and the underlying rocks, therefore chert can be used to compare trace element characteristics across the formation. Among the cherts of members 1–4 and underlying rocks, a quasi-hyperbolic correlation (Fig. 7) is observed between Y/Ho ratio and Ba, Co, Cu, Mo—metals that are typically enriched in hydrothermal fluids that have circulated through hot crustal rocks.

This correlation could be approximated by mixing of hydrothermal and marine fluids—a scenario that is consistent with the field observation of veins terminating in bedded cherts directly overlying the marine deposits of member 2. In this interpretation, the samples with the highest Y/Ho ratio represent the most 'seawater-like' chemistry and the samples with the highest Co concentrations have the strongest hydrothermal influence.

The difficulty with attempting to model mixing of ambient seawater and at least one if not several hydrothermal input sources is that none of the fluid compositions is known, and the various cherts must have formed over a range of pH, T and salinity conditions. Notwithstanding this limitation, we note that this is the first example of an Archaean sedimentary environment that appears to preserve evidence for venting of hydrothermal fluids (including high T fluids) into ambient ocean water. A higher hydrothermal flux to the ocean has thus far only been inferred indirectly from many aspects of marine sediments, including the unradiogenic Sr-isotope composition (e.g. Shields, 2007), the elevated Eu anomaly (Derry and Jacobsen, 1990) and, by some (e.g. Kasting et al., 2006), the different O-isotope composition of the Archaean ocean. For this reason, we believe that the data presented here are important.

From a quantitative perspective, strictly speaking, the hyperbolical relationships can only be used to infer that ambient seawater must have had REE and metal chemistry more extreme than the chert with the lowest metal content. Conversely, the REE patterns with the highest metal content most closely resemble those of the hydrothermal fluids that were vented into the depositional environment. We constructed a binary mixing curve to test how far the range of chemistries of the entire chert suite could be described by only two major REE and metal sources (ambient seawater and one hydrothermal fluid). According to this reasoning, seawater and hydrothermal endmembers were calculated as the average of the three samples with the highest Y/Ho and Co concentrations, respectively. A hypothetical mixing hyperbola can then be calculated between seawater and hydrothermal endmember compositions. It is important to note that because this curve was not calculated from actual fluid endmembers and because the scavenging efficiencies from the various fluid mixtures was likely variable, the curvature of the hyperbola is not an accurate reflection of a true binary fluid mixing curve. The concentrations of different elements in the geological samples are plotted against the hypothetical mixing curves for the selected elements. Fig. 7a–g show cherts from members 2–4 and underlying rocks plotted against hypothetical mixing hyperbolae for seven different metals vs. Y/Ho. All the cherts generally plot close to the hyperbolae, with member 2 cherts occurring at the seawater end of the curve, member 4 cherts at the hydrothermal end, and member 3 and underlying cherts in between. If the most metal-rich member 4 cherts precipitated from a hydrothermal fluid (and can thus be used to approximate the hydrothermal endmember), this appears to be a semi-quantitative confirmation that the trace element compositions across the suite of cherts represent different mixtures of ambient seawater and hydrothermal fluids. This is consistent with the independent sedimentological interpretations of the depositional facies from which the samples were selected (Allwood et al., 2006a).

6.3. Member 2 trace element chemistry

Notwithstanding the observation that member 2 cherts and dolomites have very similarly shaped REE+Y patterns, there is some variation. Because there is a high degree of covariance between the different aspects of the member 2 REE+Y features, closer inspection is warranted.

The first important observation is that there is a clear linear correlation between Y/Ho and La anomaly: the samples with the highest Y/Ho also having the strongest La anomaly. These latter samples appear in every aspect fully marine in character and are completely comparable to Archean open ocean seawater. The samples with less pronounced marine characteristics were either directly contaminated with clastic or volcaniclastic debris, or formed in water where open marine seawater mixed with estuarine and/or hydrothermal waters, both of which have lower or absent Y and La excesses. The correlation between Y/Ho and La anomaly can be approximated with a mixing hyperbola that was calculated using the two samples with the highest Y/Ho values as the open seawater endmember and the carbonate sample with the highest Th content (member 1 carbonate matrix) as the contaminant. Thorium is an element typically enriched in continental crust and can be used as an indicator of terrigenous contamination. Fig. 7h shows the hypothetical Y/Ho vs. Th hyperbola plotted with the Y/Ho vs. Th data for each of the samples. The trend among the samples approximates the hypothetical mixing curve quite well, indicating that the carbonates were derived from seawater with variable amounts of terrigenous (shale) contamination. Dilution of the open marine REE+Y signature is also possible in the absence of actual terrigenous sediment contamination, as demonstrated by previous studies of subrecent carbonate (coral aragonite, Wyndham et al. 2004) and late Archean carbonate (microbial limestone, Kamber and Webb, 2001). In those cases, REE+Y patterns with suppressed La and Y excesses are found in very proximal settings or even in estuaries. However, in the presently studied samples the absolute Th concentrations argue strongly for contamination by actual detritus. The greatest shale contamination occurs in the dolomite matrix of member 1, which is consistent with the fact that the

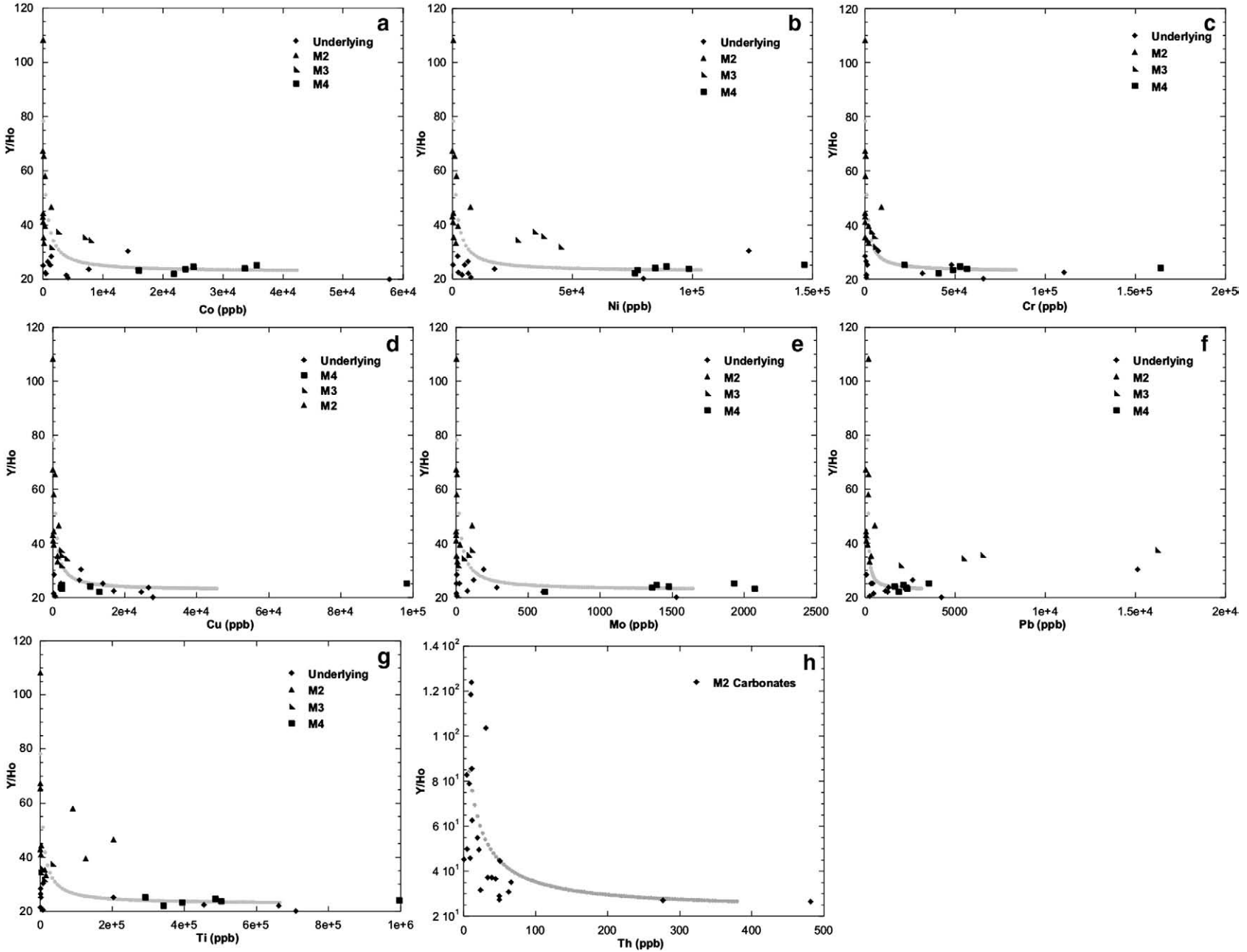

Fig. 7. Strelley Pool Formation samples plotted against the theoretical mixing hyperbolae. (a–g) Chert samples plotted with mixing hyperbola between marine and hydrothermal endmembers for a variety of metals vs. Y/Ho. (h) Dolomite samples of member 2 plotted with mixing hyperbola between marine and terrigenous endmembers. Increasing terrigenous contamination to the right. The two data point furthermost to the right are samples from the matrix of member 1 conglomerate.

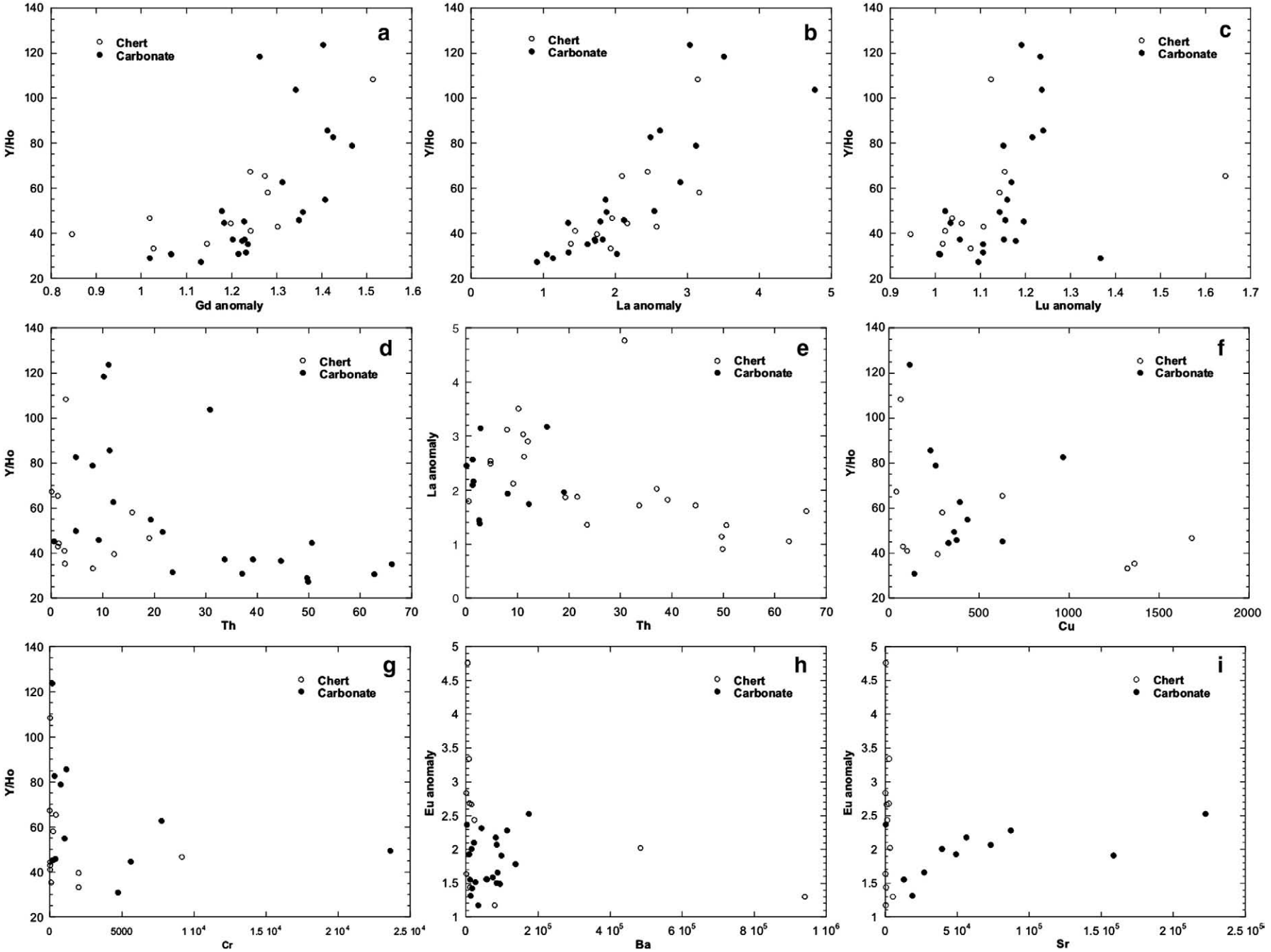

Fig. 8. Correlation trends among chert and dolomite samples from member 2. Abundances in parts per billion.

dolomite is the matrix of a poorly-sorted siliciclastic rock. Notably, however, the 'shale' could consist of siliciclastic or volcaniclastic debris, and – as with the chert mixing hyperbola – the steep curve indicates that only a small amount of contamination was required to suppress the seawater characteristics. Therefore, the variable Y/Ho ratios among the carbonate samples probably represent only a very small degree of siliciclastic or volcaniclastic contamination.

Whereas shale contamination can account for most of the REE+Y variability, the scatter around the two endmember mixing hyperbolae and the variability of Y/Ho (and other REE+Y characteristics) in chert and dolomite samples suggests that there were additional minor inputs to chemistry of chert and carbonate in member 2. In particular, the minor hydrothermal contamination noted in member 2 cherts (described above) probably influenced the carbonate as well, given the intimate spatial association of the carbonate and chert. That is, the chemistry of the whole member 2 chert+carbonate system may represent a 3-endmember continuum centred on seawater with small inputs from both terrigenous and hydrothermal sources. In that case, the carbonate and chert samples should show similar chemical characteristics – allowing for the crystallographically controlled preferential uptake of some elements in one mineral or the other – with shared trends among elements and ratios characterizing the various inputs.

Many such informative trends are observed, with a number of strong correlations among both chert and dolomite samples attesting to minor hydrothermal and terrigenous inputs in a dominantly marine system. The common marine influence is seen in dolomite and chert correlations between: 1) Y/Ho and La anomaly; 2) Y/Ho and Lu anomaly; 3) Y/Ho and Gd anomaly; and 4) Lu anomaly and Gd anomaly (Fig. 8a–c). The terrigenous contamination previously noted in the carbonates is paralleled in the cherts, as shown by a common general anti-correlation between Y/Ho vs. Th and La anomaly vs. Th (Fig. 8d, e). If the contaminant was relatively rich in Cr, as could be imagined for mafic volcaniclastics or even ordinary Early Archean clay (e.g. Condie, 1993) the weak anti-correlation between Y/Ho and Cr (Fig. 6g) could also be interpreted as incorporation of detritus. However, a similar trend is observed for Y/Ho vs. Cu, which is more consistent with admixture of low Y/Ho, Cu-bearing hydrothermal fluids.

A hydrothermal input is supported by positive correlation between the extent of the Eu anomaly and Ba and Sr concentrations (Fig. 8h, i). Although the trendline for the Eu anomaly-Sr correlation is distinctly different between chert and carbonate (Fig. 8i), the difference can be attributed to the fact that strontium readily substitutes for calcium and magnesium in carbonate minerals but has no crystallographic site to substitute in silica.

The correlation between Eu anomaly and Ba and Sr concentrations (Fig. 6i) could be interpreted in two ways. Firstly, the samples with stronger positive Eu anomaly could have been precipitated from fluids with a slightly stronger hydrothermal influence, as suggested by the positive correlation with Sr and Ba. Alternatively, the correlation of Eu anomaly with Sr concentration could reflect a chemocline between deeper marine waters (rich in Sr and with high Eu anomalies) and shallower water (with more terrigenous chemistries, lower Sr concentrations and no significant Eu anomaly) as described by Kamber and Webb (2001) for Late Archean stromatolites of the Gamohaan Formation (see e.g. Lawrence and Kamber (2006), for the conservative behaviour of Sr). In the context of the present dataset, however, the hydrothermal explanation is more likely because the Eu anomaly does not correlate with other REE+Y features. This is most readily explained by admixture of a small proportion of a hydrothermal fluid with a very strong Eu anomaly, which would not influence the remaining REE+Y pattern significantly at all.

Thus, most trace elements and REE+Y characteristics and ratios in carbonates and cherts of member 2 contain consistent information, suggesting that both were derived from related fluid sources, which were predominantly marine in origin with variable but relatively small inputs from terrigenous and hydrothermal sources.

7. Conclusions

The present study demonstrates the quality and quantity of palaeoenvironmental information that can be obtained from the REE chemistry of Early Archean sedimentary rocks when combined with careful sedimentological reconstruction. Subtle palaeoenvironmental variations that were recorded in the sedimentary carbonates and cherts of the Strelley Pool Formation c.3.45 billion years ago have survived to the present day, and are detectable in sub-microgram-sized samples using the experimental procedures described herein. Having established the reliability and primary origin of the data, several significant conclusions may be drawn regarding the changing palaeoenvironmental conditions during deposition of the Strelley Pool Formation.

The shale-normalized REE+Y patterns of cherts in the Strelley Pool Formation in the study area record fluctuating hydrothermal and marine palaeoenvironmental inputs through time. Initial mixed hydrothermal inputs (observed in underlying cherts and preserved in redeposited chert clasts in member 1 conglomerate) gave way to marine conditions that prevailed during the formation of a stromatolite reef (member 2). REE+Y and other trace element signatures in member 2 indicate that the chert and carbonate were derived from marine water, with variable but small amounts of terrigenous contamination and hydrothermal fluid advection. The close alignment of carbonate and chert trace element chemistry demonstrates that both mineral phases were derived from the same marine fluids, and neither are diagenetic replacement phases derived from, for example, later intrusive hydrothermal fluids. The demise of the stromatolite reef coincided with resumed stronger hydrothermal input in member 3 black cherts. Hydrothermal influence then dominated through deposition of member 4 black cherts.

We are able to semi-quantitatively estimate the hydrothermal and marine palaeoenvironmental inputs at different stages of deposition by the use of binary mixing models. According to these calculations, the cherts through the formation represent mixtures of hydrothermal and marine endmembers: member 2 has 90% or more of the seawater endmember; whereas member 3 and underlying cherts have 0–90%; and member 4 has 0–50%.

Importantly, the main variations observed in the degree of marine, hydrothermal and terrigenous influence are consistent with a diverse array of independent sedimentological indicators: for example, the cherts with the strongest hydrothermal REE+Y signatures overlie hydrothermal black chert 'feeder' veins, show zones of phreatomagmatic brecciation, have intercalated tuff beds and are conformably overlain by basalt; whereas chert and carbonate associated with stromatolites and peritidal facies associations have marine REE signatures (Allwood et al., 2006a). Thus, REE+Y chemistry of carbonates and cherts of the Strelley Pool Formation underscore the relationship between a brief hiatus in the hydrothermal and volcanic activity that prevailed on the Pilbara Craton in the Early Archean, and the development of Earth's oldest preserved carbonate platform and stromatolites in marine conditions. As far as we can determine, this type of geochemical modeling of changing environmental conditions has not before been achieved in rocks of Archean age.

Acknowledgements

We are grateful to the Geological Survey of Western Australia for the generous field support and particularly to Arthur Hickman for his helpful discussions. We also gratefully acknowledge: Alan Greig for the ICPMS laboratory assistance; John Grotzinger for the discussions and use of facilities at Caltech; and Andrew Knoll, Stanley Awramik, Max Coleman, Kath Grey, Paul Knauth, Dawn Sumner and Woodward Fischer for their helpful discussions. Allwood is supported by the NASA Postdoctoral Program. Kamber acknowledges support from the CRC. Part of the research described in this paper was carried out at the

Jet Propulsion Laboratory, California Institute of Technology, under a contract with the National Aeronautics and Space Administration.

Appendix A. Supplementary data

Supplementary data associated with this article can be found, in the online version, at doi:10.1016/j.chemgeo.2009.11.013.

References

Alexander, B.W., Bau, M., Andersson, P., Dulski, P., 2008. Continentally-derived solutes in shallow Archean seawater: rare earth element and Nd isotope evidence in iron from the 2.9 Ga Pongola Supergroup, South Africa. Geochimica et Cosmochimica Acta 72, 378–394.

Alibert, C., McCulloch, M.T., 1993. Rare earth element and neodymium isotopic compositions of the banded iron-formations and associated shales from Hamersley, western Australia. Geochimica et Cosmochimica Acta 57, 187–204.

Allwood, A.C., Walter, M.R., Kamber, B.S., Marshall, C.P., Burch, I.W., 2006a. Stromatolite reef from the Early Archaean era of Australia. Nature 441, 714–718.

Allwood, A.C., Walter, M.R., Marshall, C.P., 2006b. Raman spectroscopy reveals thermal palaeoenvironments of c.3.5 billion-year-old organic matter. Journal of Vibrational Spectroscopy 41 (2), 190–197.

Allwood, A.C., Walter, M.R., Burch, I.W., 2007a. Stratigraphy and facies of the 3.43 Ga Strelley Pool chert in the Southwest North Pole Dome. Western Australia Geological Survey Record 2007/11.

Allwood, A.C., Walter, M.R., Burch, I.W., Kamber, B.S., 2007b. 3.43 billion-year-old stromatolite reef from the Pilbara Craton of Western Australia: ecosystem-scale insights to early life on Earth. Precambrian Research 158 (3–4), 198–227.

Allwood, A.C., Grotzinger, J.P., Knoll, A.H., Burch, I.W., Anderson, M.S, Coleman, M.L., Kanik, I., 2009. Controls on development and diversity of Early Archean stromatolites. Proceedings of the National Academy of Sciences 106, 9548–9555.

Awramik, S.M., Margulis, L., Barghoorn, E.S., 1976. Evolutionary processes in the formation of stromatolites. In: Walter, M.R. (Ed.), Stromatolites. Elsevier, Amsterdam, pp. 149–162.

Banner, J.L., Hansen, G.N., 1990. Calculation of simultaneous isotopic and trace element variations during water–rock interaction with applications to carbonate diagenesis. Geochimica et Cosmochimica Acta 54, 3123–3137.

Bau, M., 1996. Controls on the fractionation of isovalent trace elements in magmatic and aqueous systems: evidence from Y/Ho, Zr/Hf, and lanthanide tetrad effect. Contributions to Mineralogy Petrology 123, 323–333.

Bau, M., 1999. Scavenging of dissolved yttrium and rare earths by precipitating iron oxyhydroxide; experimental evidence for Ce oxidation, Y-Ho fractionation, and lanthanide tetrad effect. Geochimica et Cosmochimica Acta 63, 67–77.

Bau, M., Moller, P., 1993. Rare earth element systematics of the chemically precipitated component in early precambrian iron formations and the evolution of the terrestrial atmosphere–hydrosphere–lithosphere system. Geochimica et Cosmochimica Acta 57, 2239–2249.

Bau, M., Dulski, P., 1996. Distribution of yttrium and rare-earth elements in the Penge and Kuruman iron-formations, Transvaal Supergroup, South Africa. Precambrian Research 79, 37–55.

Bau, M., Dulski, P., 1999. Comparing yttrium and rare earths in hydrothermal fluids from the Mid-Atlantic Ridge: implications for Y and REE behaviour during near-vent mixing and for the Y/Ho ratio of Proterozoic seawater. Chemical Geology 155, 77–90.

Bau, M., Alexander, B., 2006. Preservation of primary REE patterns without Ce anomaly during dolomitization of Mid-Paleoproterozoic limestone and the potential re-establishment of marine anoxia immediately after the "Great Oxidation Event". South African Journal of Geology 109, 81–86.

Bau, M., Koschinsky, A., 2009. Oxidative scavenging of cerium on hydrous Fe oxide: evidence from the distribution of rare earth elements and yttrium between Fe oxides and Mn oxides in hydrogenetic ferromanganese crusts. Geochemical Journal 43, 37–47.

Bau, M., Usui, A., Pracejus, B., Mita, N., Kanai, Y., Irber, W., Dulski, P., 1999. Geochemistry of low-temperature water–rock interaction: evidence from natural waters, andesite, and iron-oxyhydroxide precipitates at Nishiki-numa iron-spring, Hokkaido, Japan. Chemical Geology 151, 293–307.

Bolhar, R., Kamber, B.S., Webb, G.E., Collerson, K.D., 2004. Trace element fingerprints of early Archaean hydrogenous carbonates; a possible test for the presence of an ancient Martian ocean. Abstracts – Geological Society of Australia 73, 5.

Buick, R., Thornett, J.R., McNaughton, N.J., Smith, J.B., Barley, B.E., Savage, M., 1995. Record of emergent continental crust ~3.5 Billion years ago in the Pilbara Craton of Australia. Nature 441, 574–577.

Condie, K.C., 1993. Chemical composition and evolution of the upper continental crust: contrasting results from surface samples and shales. Chemical Geology 104, 1–37.

Derry, L.A., Jacobsen, S.B., 1990. The chemical evolution of Precambrian seawater; evidence from REEs in banded iron formations. Geochimica et Cosmochimica Acta 54, 2965–2977.

DiMarco, M.J., Lowe, D.R., 1989. Stratigraphy and sedimentology of an early Archean felsic volcanic sequence, eastern Pilbara Block, Western Australia, with special reference to the Duffer Formation and implications for crustal evolution. Precambrian Research 44, 147–169.

Douville, E., Bienvenu, P., Charlou, J.L., Donval, J.P., Fouquet, Y., Appriou, P., Gamo, T., 1999. Yttrium and rare earth elements in fluids from various deep-sea hydrothermal systems. Geochimica et Cosmochimica Acta 63, 627–643.

Eggins, S.M., Woodhead, J.D., Kinsley, L.P.J., Mortimer, G.E., Sylvester, P., McCulloch, M. T., Hergt, J.M., Handler, M.R., 1997. A simple method for the precise determination of > or = 40 trace elements in geological samples by ICPMS using enriched isotope internal standardisation. Chemical Geology 134, 311–326.

Herdianita, N.R., Browne, P.R.L., Rodgers, K.A., Campbell, K.A., 2000. Mineralogical and textural changes accompanying ageing of silica sinter. Mineralium Deposita 35 (1), 48–62.

Hickman, A.H., 2008. Regional review of the 3426–3350 Ma Strelley Pool Formation, Pilbara Craton, Western Australia. Western Australia Geological Survey Record 2008/15.

Hofmann, H.J., 1973. Stromatolites; characteristics and utility. Earth Science. Reviews 9, 339–373.

Hoffman, H.J., Grey, K., Hickman, A.H., Thorpe, R.I., 1999. Origin of 3.45 Ga coniform stromatolites in Warrawoona Group, Western Australia. GSA Bulletin 111, 1256–1262.

Jones, B., Renaut, R., 2007. Microstructural changes accompanying the opal-A to opal-CT transition: new evidence from the siliceous sinters of Geysir, Haukadalur. Iceland Sedimentology 54, 921–948.

Kamber, B.S., Webb, G.E., 2001. The geochemistry of Late Archean microbial carbonate: implications for ocean chemistry and continental erosion history. Geochimica et Cosmochimica Acta 65, 2509–2525.

Kamber, B.S., Greig, A., Schoenberg, R., Collerson, K.D., 2003. A refined solution to Earth's hidden niobium; implications for evolution of continental crust and mode of core formation. Precambrian Research 126, 289–308.

Kamber, B.S., Bolhar, R., Webb, G.E., 2004. Geochemistry of late Archaean stromatolites from Zimbabwe; evidence for microbial life in restricted epicontinental seas. Precambrian Research 132, 379–399.

Kamber, B.S., Greig, A., Collerson, K.D., 2005. A new estimate for the composition of weathered young upper continental crust from alluvial sediments, Queensland, Australia. Geochimica et Cosmochimica Acta 69, 1041–1058.

Kasting, J.F., Howard, M.T., Wallmann, K., Veizer, J., Shields, G., Jaffres, J., 2006. Paleoclimates, ocean depth, and the oxygen isotopic composition of seawater. Earth and Planetary Science Letters 252, 82–93.

Kastner, M., Keene, J.B., Gieskes, J.M., 1977. Diagenesis of siliceous oozes — I. Chemical controls on the rate of opal-A to opal-CT transformation — an experimental study. Geochimica et Cosmochimica Acta 41, 1041–1059.

Klinkhammer, G.P., Elderfield, H., Edmond, J.M., Mitra, A., 1994. Geochemical implications of rare earth element patterns in hydrothermal fluids from mid-ocean ridges. Geochimica et Cosmochimica Acta 58, 5105–5113.

Kulaksiz, S., Bau, M., 2007. Contrasting behaviour of anthropogenic gadolinium and natural rare earth elements in estuaries and the gadolinium input into the North Sea. Earth and Planetary Science Letters 260, 361–371.

Lawrence, M.G., Kamber, B.S., 2006. Behaviour of the rare earth elements during estuarine mixing — revisited. Marine Chemistry 100, 147–161.

Lee, J.H., Byrne, R.H., 1992. Examination of comparative rare earth element complexation behavior using linear free-energy relationships. Geochimica et Cosmochimica Acta 56, 1127–1137.

Lindsay, J.F., Brasier, M.D., McLoughlin, N., Green, O.R., Fogel, M., Steele, A., Mertzman, S.A., 2005. The problem of deep carbon; an Archean paradox. Precambrian Research 143, 1–22.

Lowe, D.R., 1980. Stromatolites 3,400–3,500 Myr old from the Archean of Western Australia. Nature 284, 441–443.

Lowe, D.R., 1983. Restricted shallow-water sedimentation of early Archean stromatolitic and evaporitic strata of the Strelley Pool Formation, Pilbara Block, Western Australia. Precambrian Research 19, 239–283.

Lynne, B.Y., Campbell, K.A., Moore, J.N., Browne, P.R.L., 2005. Diagenesis of 1900-year-old siliceous sinter (opal-A to quartz) at Opal Mound, Roosevelt Hot Springs, Utah, USA. Sedimentary Geology 179, 249–278.

Marx, S.K., Kamber, B.S., McGowan, H.A., 2005. Provenance of long-travelled dust determined with ultra-trace-element composition: a pilot study with samples from New Zealand glaciers. Earth Surface Processes and Landforms 30, 699–716.

Nozaki, Y., Zhang, J., Amakawa, H., 1997. The fractionation between Y and Ho in the marine environment. Earth and Planetary Science Letters 148, 329–340.

Nothdurft, L.D., Webb, G.E., Kamber, B.S., 2004. Rare earth element geochemistry of Late Devonian reefal carbonates, Canning basin, Western Australia: confirmation of a seawater REE proxy in ancient limestones. Geochimica et Cosmochimica Acta. 68, 263–283.

Shields, G., 2007. The marine carbonate and chert isotope records and their implications for tectonics, life and climate on the early earth. In: Van Kranendonk, M.J. (Ed.), Earth's Oldest Rocks. Developments in Precambrian Geology. Elsevier, Amsterdam, pp. 971–983.

Sholkovitz, E.R., Schneider, D.L., 1991. Cerium redox cycles and rare earth elements in the Sargasso Sea. Geochimica et Cosmochimica Acta 55, 2737–2743.

Smith, D.K., 1998. Opal, cristobalite, and tridymite: noncrystallinity versus crystallinity, nomenclature of the silica minerals and bibliography. Powder Diffraction 13, 2–19.

Sugitani, K., 1992. Geochemical characteristics of Archean cherts and other sedimentary rocks in the Pilbara Block, Western Australia; evidence for Archean seawater enriched in hydrothermally-derived iron and silica. Precambrian Research 57, 21–47.

Taylor, S.R., McLennan, S.M., 1985. The Continental Crust: Its Composition and Evolution. Blackwell Scientific Pub, Palo Alto, CA. 328 pp.

Van Kranendonk, M.J., Pirajno, F., 2004. Geochemistry of metabasalts and hydrothermal alteration zones associated with c. 3.45 Ga chert and barite deposits: implications

for the geological setting of the Warrawoona Group, Pilbara Craton, Australia. Geochemistry: Exploration, Environment, Analysis 4, 253–278.
Van Kranendonk, M.J., Hickman, A.H., Smithies, R.H., Nelson, D.R., Pike, G., 2002. Geology and tectonic evolution of the Archaean North Pilbara terrain, Pilbara Craton, Western Australia. Economic Geology 97, 695–732.
Van Kranendonk, M.J., Webb, G.E., Kamber, B.S., 2003. Geological and trace element evidence for a marine sedimentary environment of deposition and biogenicity of 3.45 Ga stromatolitic carbonates in the Pilbara Craton, and support for a reducing Archaean ocean. Geobiology 1, 91–108.
Wheat, C.G., Mottl, M.J., Rudnicki, M., Candela, P.A., 2002. Trace element and REE composition of a low-temperature ridge-flank hydrothermal spring. Geochimica et Cosmochimica Acta 66, 3693–3705.
Wyndham, T., McCulloch, M., Fallon, S., Alibert, C., 2004. High resolution coral records of rare earth elements in coastal seawater: biogeochemical cycling and a new environmental proxy. Geochimica et Cosmochimica Acta 68, 2067–2080.